Measurement of Granular Temperature and Stresses in Risers

Mehmet Tartan and Dimitri Gidaspow
Chemical and Environmental Engineering Dept., Illinois Institute of Technology, Chicago, IL 60616

DOI 10.1002/aic.10192
Published online in Wiley InterScience (www.interscience.wiley.com).

Detailed experimental velocity, particle concentration, and stresses for flow of particles in a vertical pipe, riser are needed for verification of various CFD models for multiphase flow. This is the principle-unsolved task of the Fluid Dynamics Multiphase Flow Consortium, organized by Dow Chemical Company. This study provides such information for flow of 530 μm glass beads in the fully developed flow region of a 7 m symmetric riser with a splash plate. Instantaneous particle-velocity distributions were obtained using a particle velocity imaging technique, and a probe inserted into the riser, while the particle concentrations were measured with a gamma-ray densitometer. Time-averaged particle-velocity distributions can be well represented by a parabolic- velocity distribution, with the mean velocity obtained from flux divided by the measured bulk density. The flow is very anisotropic. The radial granular-temperature profiles agree with an analytical expression similar to the thermal-temperature distribution in Poiseuille flow with viscous heat generation. A numerical solution for the standard isotropic model developed shows that the approximations made in the analytical solutions are reasonable. In the core, the normal Reynolds stresses are much smaller than the velocity averaged particle stresses, whereas near the wall the time averaged normal Reynolds stresses are large. © 2004 American Institute of Chemical Engineers *AIChE J,* 50: 1760–1775, 2004
Keywords: fluidization, gas-particle flow, kinetic theory, Reynolds stresses

Introduction

Quantitative understanding of the hydrodynamics of fluidization is needed for the design and scale-up of efficient new reactors in the petroleum, chemical, and in the electric power industries (Avidan et al., 1990; Squires et al., 1985; Berruti et al., 1995; Sinclair, 1997). For example, it was only a decade ago that the oil industry using gamma ray techniques (Sun and Koves, 1998) learned that their large diameter risers operate in the core-annular regime: the core is very dilute. The core-annular structure leads to two main problems: (1) insufficient gas-solid contact, and (2) back-mixing due to nonuniform radial distributions (Jin et al. 1997). Our simulation (Therdthianwong and Gidaspow, 1994) of sorption of sulfur dioxide by calcined dolomite in a Pyropower CFB loop shows that the pollutant gas is fully removed in the annulus, but not at the center of the riser. This unfavorable radial volume fraction distribution of solids in the riser has led to considerations of new schemes of contacting for a refinery of the 21st Century.

There is a worldwide effort (Australia: CSIRO; Canada: Grace et al., 1990; China: Kwauk et al., 1986; England: Rhodes et al. 1989; France: Galtier et al. 1989; Azzi et al., 1991; Germany: Werther et al., 1990; Italy: Arena et al. 1989; Japan: Tsuji et al. 1998; Netherlands: Nieuwiand et al., 1996; Norway: Samuelsberg and Hjertager, 1996; USA: Bader et al. 1988; Weinstein et al., 1986; Sinclair and Jackson, 1989; Sinclair, 1997; Pita and Sundaresan, 1991; Zhang et al. 1996, Benyahia et al. 1998) to understand the hydrodynamics of dense vertical gas-solid flow in a pipe usually referred to in the literature as circulating fluidized bed, or riser flow. Earlier, this flow regime was called fast fluidization, to distinguish it from the slow bubbling fluidization (Squires et al., 1985; Yerushalmi, 1986).

Correspondence concerning this article should be addressed to D. Gidaspow at gidaspow@iit.edu.

Table 1. Hydrodynamic Model

Gas-phase continuity	$\frac{\partial}{\partial t}(\epsilon_g\rho_g) + \nabla\cdot(\epsilon_g\rho_g\mathbf{v}_g) = 0$
Solid-phase continuity	$\frac{\partial}{\partial t}(\epsilon_s\rho_s) + \nabla\cdot(\epsilon_s\rho_s\mathbf{v}_s) = 0$
Gas-phase momentum	$\frac{\partial}{\partial t}(\epsilon_g\rho_g\mathbf{v}_g) + \nabla\cdot(\epsilon_g\rho_g\mathbf{v}_g\mathbf{v}_g) = -\nabla P_g + \nabla\cdot\mathbf{T}_g + \rho_g\mathbf{g} + \beta(\mathbf{v}_s - \mathbf{v}_g)$
Solid-phase momentum	$\frac{\partial}{\partial t}(\epsilon_s\rho_s\mathbf{v}_s) + \nabla\cdot(\epsilon_s\rho_s\mathbf{v}_s\mathbf{v}_s) = \nabla\cdot\mathbf{T}_s + \epsilon_s(\rho_s - \rho_g)\mathbf{g} - \beta(\mathbf{v}_s - \mathbf{v}_g)$
Solid-phase fluctuating energy	$\frac{3}{2}\left[\frac{\partial}{\partial t}(\epsilon_s\rho_s\theta) + \nabla\cdot(\epsilon_s\rho_s\theta\mathbf{v}_s)\right] = \mathbf{T}_s : \nabla\mathbf{v}_s + \nabla\cdot(\kappa_s\nabla\theta) - \gamma_s$
Gas-phase stress tensor	$\mathbf{T}_g = 2\epsilon_g\mu_g\left\{\frac{1}{2}[\nabla\mathbf{v}_g + (\nabla\mathbf{v}_g)^T] - \frac{1}{3}(\nabla\cdot\mathbf{v}_g)\mathbf{I}\right\}$
Solid-phase stress tensor	$\mathbf{T}_s = (-P_s + \xi_s\nabla\cdot\mathbf{v}_s)\mathbf{I} + 2\mu_s\left\{\frac{1}{2}[\nabla\mathbf{v}_s + (\nabla\mathbf{v}_s)^T] - \frac{1}{3}(\nabla\cdot\mathbf{v}_s)\mathbf{I}\right\}$
Solid pressure	$P_s = \epsilon_s\rho_s\theta[1 + 2(1 + e)g_o\epsilon_s]$
Bulk solid viscosity	$\xi_s = \frac{4}{3}\epsilon_s^2\rho_s d_p(1 + e)g_o\sqrt{\frac{\theta}{\pi}}$
Solid viscosity	$\mu_s = \frac{10\sqrt{\pi}\rho_s d_p\sqrt{\theta}}{96(1 + e)g_o}\left[1 + \frac{4}{5}(1 + e)g_o\epsilon_s\right]^2 + \frac{4}{5}\epsilon_s^2\rho_s d_p(1 + e)g_o\sqrt{\frac{\theta}{\pi}}$
Granular conductivity	$\kappa_s = \frac{150\sqrt{\pi}\rho_s d_p\sqrt{\theta}}{384(1 + e)g_o}\left[1 + \frac{6}{5}(1 + e)g_o\epsilon_s\right]^2 + 2\epsilon_s^2\rho_s d_p(1 + e)g_o\sqrt{\frac{\theta}{\pi}}$
Collisional energy dissipation	$\gamma_s = 3(1 - e^2)\epsilon_s^2\rho_s g_o\theta\left(\frac{4}{d_p}\sqrt{\frac{\theta}{\pi}} - \nabla\cdot\mathbf{v}_s\right)$
Drag coefficient $\epsilon_g \geq 0.8$:	$\beta = \frac{3}{4}C_d\frac{\epsilon_s\rho_g\lvert\mathbf{v}_g - \mathbf{v}_s\rvert}{d_p}\epsilon_g^{-2.65}$
$\mathrm{Re}_s = \frac{\epsilon_g\rho_g d_p\lvert\mathbf{v}_g - \mathbf{v}_s\rvert}{\mu_g}$	$C_d = \frac{24}{\mathrm{Re}_s}(1 + 0.15\mathrm{Re}_s^{0.687})$; $\mathrm{Re}_s < 1{,}000$ $C_d = 0.44$; $\mathrm{Re}_s \geq 1{,}000$
Drag coefficient $\epsilon_g < 0.8$:	$\beta = 150\frac{\epsilon_s^2\mu_g}{\epsilon_g^2 d_p^2} + 1.75\frac{\rho_g\epsilon_s\lvert\mathbf{v}_g - \mathbf{v}_s\rvert}{d_p\epsilon_g}$

Recently, Berruti et al. (1995) have reviewed the hydrodynamics of circulating fluidized-bed risers.

Multiphase flow models were reviewed by Shook and Roco (1991), Gidaspow (1994); Sinclair (1997); Crowe (1996, 1998), and Jackson (2000) in the U.S., by Hjertager et al. (1998), from Norway, by Kuipers et al. (1998) from Holland and by Enwald et al. (1996) from Sweden. Different approaches to the computation (Kashiva et al. 2000; Gidaspow, 2000; Sundaresan, 2000; Smith et al. 2000; Crowe, 2000) and measurement (Dudukovic, 2000) of multiphase flow turbulence were discussed at the April 2000 MFDRC meeting (Thompson). The CFD models can be used to compute Reynolds stresses, as was demonstrated by the Dudukovic group (Pan et al., 2000), with the Los Alamos CFDLIB for gas-liquid flow using PIV data obtained in L. S. Fan laboratory (Mudde et al., 1997). A similar computation was performed by Matonis et al. (2002) for gas-liquid-solid flow, and compared to IIT data.

Sinclair and Jackson (1989) were the first to analyze fully developed riser flow using kinetic theory of granular flow. They predicted the existence of the core annular regime. The analytical solution for granular temperature is a special case of that theory for elastic particles. The existence of the core-annular regime and cluster formation were computed at the same time by Gidaspow et al. (1989); Tsuo and Gidaspow (1990), and by Gidaspow et al. (1991), using a transient two-dimensional (2-D) hydrodynamic model with particle viscosity as an input, and compared to experiments of Bader et al. (1988) and Weinstein et al. (1986). Anderson et al. (1995) used a similar model for bubbling beds. Therefore, it is not necessary to use kinetic theory to compute the core-annular regime. The model of Gidaspow et al. (1989) computes turbulent oscillations, which allow the particles to migrate toward the wall, where the velocity is too small to support their weight, resulting in accumulation or even down flow. This model is, however, not in conflict with the kinetic theory model, since one can define a turbulent granular temperature as the average of the normal Reynolds stresses. The available experimental data were insufficiently

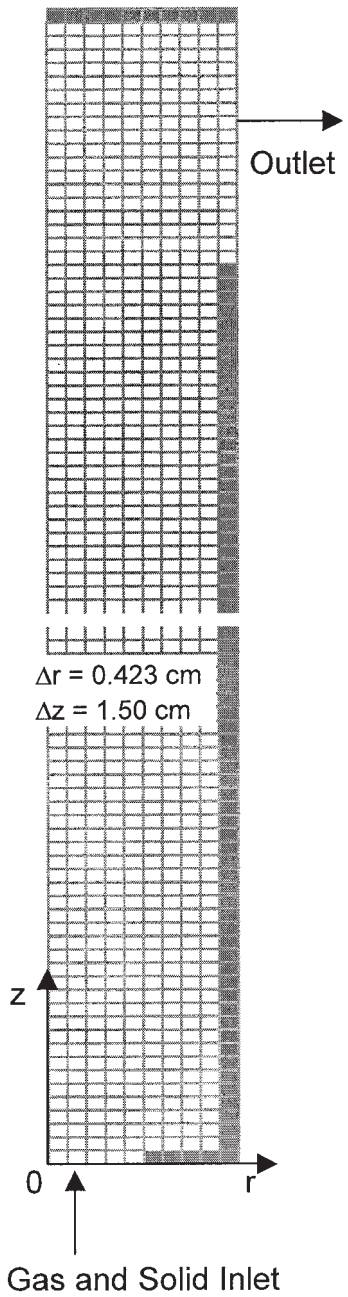

Figure 1. Riser geometry used in the simulation.

accurate to determine whether laminar or turbulent granular temperatures were more important.

Pita and Sundaresan (1991) noted the sensitivity of the Sinclair and Jackson model to the value of the restitution coefficient. Hence, their group (Dasgupta et al., 1994, 1998) added the turbulent particle oscillations using the single-phase K-epsilon approach. Hrenya and Sinclair (1997) modified this approach and computed granular temperatures, solid pressures, and viscosities for FCC particles that are close to the measurements of Gidaspow and Huilin (1996, 1998). They were computed before the publication of the experimental data. In the core of the riser Hrenya and Sinclair 's viscosities were nearly constant, as in this study, although the turbulent viscosities were somewhat higher. The data presented in this article for the Geldart group, B particles show that the particle turbulence in the core of the riser is much smaller than the laminar particle stresses. Cao and Ahmadi (1995) solved the coupled fluctuating kinetic energy equations for developed pipe flow for the particulate and the fluid phases. The coupling was through a drag-like term, similar to that in the granular temperature balance. For the simulation of Miller and Gidaspow (1992) experiment of flow of FCC particles in a riser, they obtained the observed core-annular flow and approximately the measured granular temperature before its publication (Gidaspow and Huilin, 1996). Zhang and VanderHeyden (2001, 2002) numerically solved the transient two-phase flow equations for extremely dilute flow, where the conventional kinetic theory is not applicable. They compared their computed values to measurements in the "dilute zone of a CFB" (Van den Moortel et al. 1998), more properly called the freeboard. The laser-Doppler technique used by these authors cannot be applied to measurements in the CFB due to a curtain of solids at the wall of the riser, which absorbs the laser beam. Hence, Zhang and VanderHeyden's dilute simulations, although interesting, shed no light on the behavior of a real CFB, where the particle volume fraction in the core is of the order of a few percent.

The primary purpose of this article is to present unique measurements of laminar and turbulent stresses for flow of 530 μm glass beads in the fully developed riser, constructed to give symmetric flow. The new experimental technique is capable of distinguishing between the laminar and the turbulent particle stresses. The laminar normal particle stresses are much larger than the turbulent stresses in the core of the riser, although they are of the same order of magnitude, or larger in the dense annular region. The shear stresses, as expected from theory, are zero at the center, increase almost linearly with radius, and then decrease in the dense annular region. The flow is very anisotropic, like single-phase turbulent flow in a pipe. The conventional kinetic theory of granular flow does not consider anisotropy. Nevertheless, it approximately predicts the observed laminar type flow in the center of the pipe. It also shows that the measured granular temperature can be roughly represented by an analogue of thermal temperature rise in Poiseuille flow with viscous heat generation. A more detailed analysis using the anisotropic kinetic theory of Strumendo and Canu (2002) is in progress (Strumendo et al., 2003).

Hydrodynamic Model

A kinetic theory based hydrodynamic model with Johnson and Jackson (1987) boundary conditions has been developed

Table 2. Simulation Conditions and System Properties

Riser diameter	7.62 cm
Riser inlet diameter	4.23 cm
Riser height	699 cm
Particle size	530 μm
Particle density	2.46 g/cm^3
Restitution coefficient (e)	0.98, 0.95, 0.89
Wall restitution coefficient (e_w)	0.60
Specularity coefficient (ϕ)	0.60
Solid mass flux	1.42 g/cm^2-s
Gas superficial velocity	490 cm/s (in the 7.62 cm ID tube)
Grid size ($\Delta r \times \Delta z$)	0.423 cm $\times$ 1.50 cm
Grid number	11 (radial) $\times$ 466 (axial)
Time step	5×10^{-5}

Table 3. Inlet and Outlet Conditions Used in the Simulation

Inlet Conditions					
r/R:	0.1	0.3	0.5	0.7	0.9
Gas Inlet Velocity, cm/s:	1954	1885	1797	1670	1428
Solid Inlet Velocity, cm/s:	182	167	138	94	35
Solid Volume Fraction:	0.02	0.02	0.02	0.02	0.02
Granular Temperature, cm^2/s^2:	2201	2184	2064	1673	757

Outlet Conditions

Continuous outflow

Boundary Conditions

Solid Phase (Johnson and Jackson, 1987):

$$v_{s,w} = -\frac{6\mu_s \epsilon_{s,\max}}{\sqrt{3}\pi\varphi\rho_s\epsilon_s g_o \sqrt{\theta}} \left.\frac{\partial v}{\partial n}\right|_{\text{wall}}$$

$$\theta_w = -\left(\frac{\kappa_s \theta}{\gamma_w}\right) \left.\frac{\partial \theta}{\partial n}\right|_{\text{wall}} + \frac{\sqrt{3}\pi\varphi\rho_s\epsilon_s v_{s,w}^2 g_o \theta_w^{3/2}}{6\epsilon_{s,\max}\,\gamma_w}$$

$$\text{where } \gamma_w = \frac{\sqrt{3}\pi(1-e_w^2)\epsilon_s\rho_s g_o \theta_w^{3/2}}{4\epsilon_{s,\max}}$$

Gas Phase: $v_{r,w} = v_{z,w} = 0$

by Neri and Gidaspow (2000), and applied to flow of FCC particles in the IIT riser with a U-type outlet. In this study, we have replaced the U-tube outlet with a splash plate as described in the experimental section. For the simulation, we have used cylindrical coordinates with axial symmetry. In this model, the unknown empirical parameters are the restitution coefficient for particles. The restitution coefficient for the particles with the wall was estimated from the measurements as shown in Table 4. Its average value is 0.6. This value is reasonable since the wall is softer than the particles.

Table 1 shows a summary of the basic equations. Figure 1 shows the sketch of the riser geometry used in the simulation. Table 2 gives the simulation conditions and the relevant dimensions. Table 3 shows the inlet, outlet, and boundary conditions. Unlike in the simulation of Neri and Gidaspow (2000), a parabolic solid velocity profile was used for the inlet condition.

Solids Velocity Distribution in the Core

For a developed flow, general equations given in Table 1 can be greatly simplified, as already shown in the pioneering article by Sinclair and Jackson (1989). The sum of the gas and solid momentum balances produces an equation for the mixture.

For a developed flow, this time averaged mixture momentum balance in axial direction, with negligible solid and gas-phase turbulence, can be written as follows

$$0 = \frac{d\bar{P}}{dz} + (\bar{\varepsilon}_s\rho_s + \bar{\varepsilon}_g\rho_g)\,g_z + \frac{1}{r}\frac{d}{dr}\left(r\mu_s\frac{d\bar{V}_{sz}}{dr} + r\mu_g\frac{d\bar{V}_{gz}}{dr}\right) \quad (1)$$

Table 4. Estimate of Restitution Coefficients at the Wall

Flux (kg/m^2 − s)	θ_w (cm^2/s^2)	$(d\theta/dr)_w$ (cm/s^2)	ϵ_{sw}	e_w
14.90	274	386	0.016	0.56
43.85	305	742	0.030	0.61

$$\theta_w = 0.145\,\frac{d_p}{\epsilon_s(1-e_w^2)}\left.\frac{d\theta}{dr}\right|_w$$

Since the order of magnitude of gas-phase density and viscosity is much less than solid phase, Eq. 1 can further be simplified to the following equation

$$0 = \frac{d\bar{P}}{dz} + (\bar{\varepsilon}_s\rho_s)\,g_z + \frac{1}{r}\frac{d}{dr}\left(r\mu_s\frac{d\bar{V}_{sz}}{dr}\right) \quad (2)$$

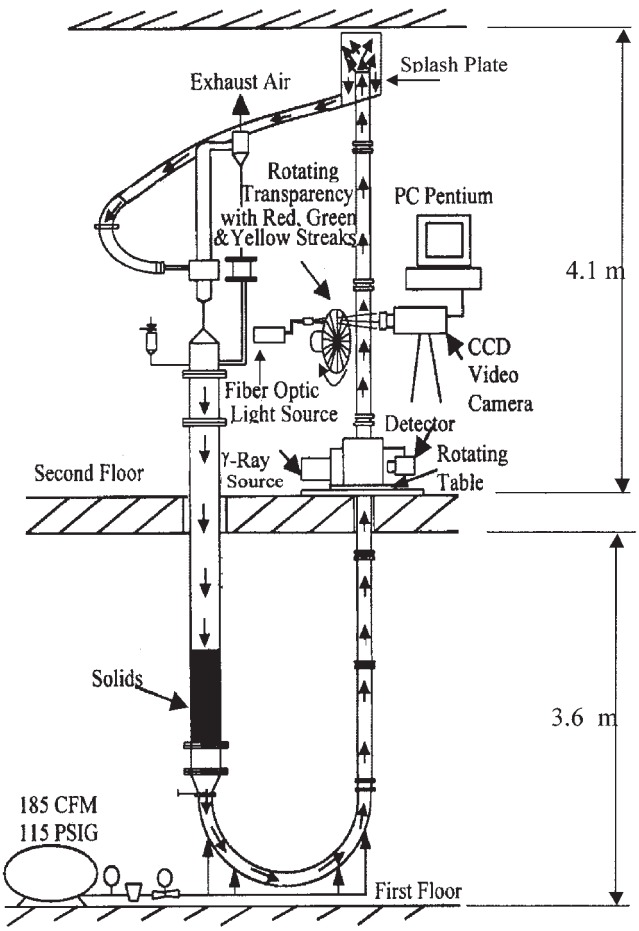

Figure 2. IIT Circulating fluidized bed with splash plate.

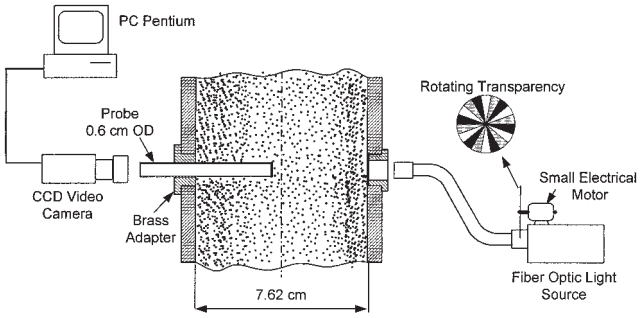

Figure 3. Particle image velocity measurement system with probe.

Next, the flow is divided into core and annular sections. For a thin annular region, an approximate analytical solution can be obtained to Eq. 2, like Poiseuille flow for a fluid with no slip at the wall

$$V_{sz} = 2V_{sM}\left(1 - \frac{r^2}{R^2}\right) \tag{3}$$

The mean velocity is obtained from the measured flux and solids volume fraction as shown below

$$V_{sM} = \frac{W_{sM}}{\epsilon_{sM}\rho_s} \tag{4}$$

Granular Temperature Analytical Solution

Table 1 provides the general granular temperature equation. In developed flow in a riser with flow of elastic particles, the granular temperature balance involves a balance between conduction and generation, as shown by Sinclair and Jackson (1989). In cylindrical coordinates it is as follows for a constant conductivity κ_s, and particle viscosity μ_s

$$-\frac{1}{r}\frac{d}{dr}\left(r\kappa_s\frac{d\theta}{dr}\right) = \mu_s\left(\frac{dV_{sz}}{dr}\right)^2 \tag{5}$$

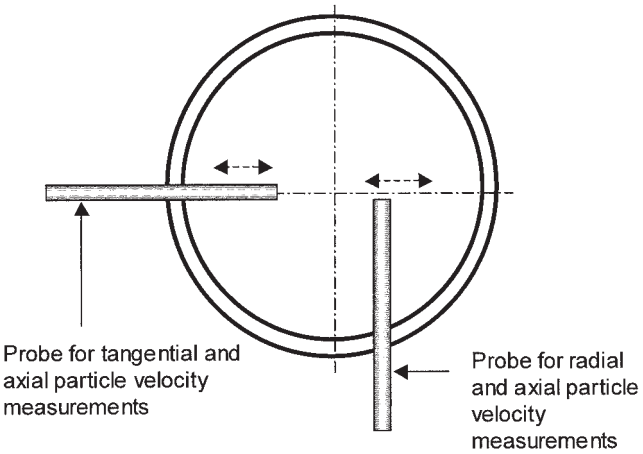

Figure 4. Probe locations for particle velocity measurements.

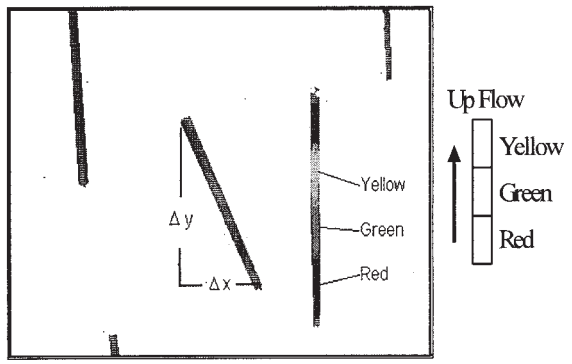

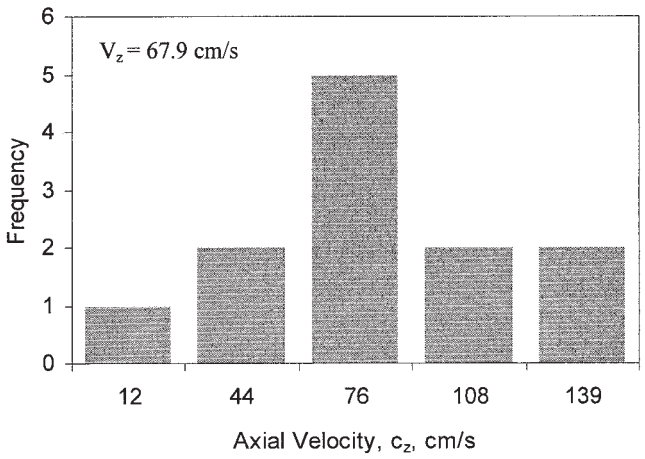

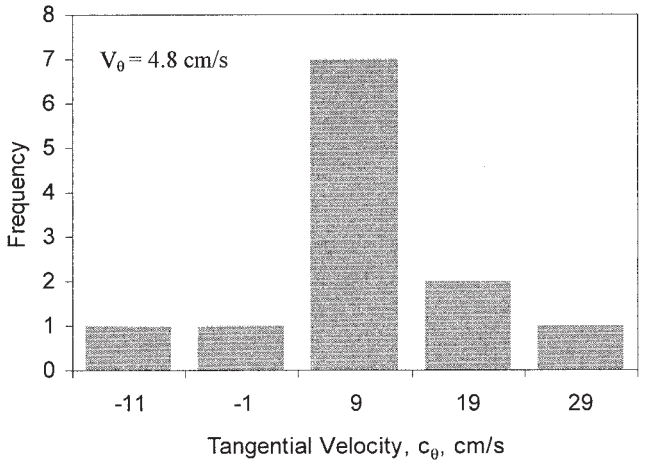

Figure 5. Typical streak images captured by CCD camera and axial, and tangential velocity distribution.

W_s = 14.2 kg/m^{2}s, U_o = 4.9 m/s, at r/R = 0.50.

As a limit, it was assumed that all dissipation occurs at the wall. We prescribe the wall granular temperature at the pipe surface $r = R$

$$\theta(R) = \theta_w \tag{6}$$

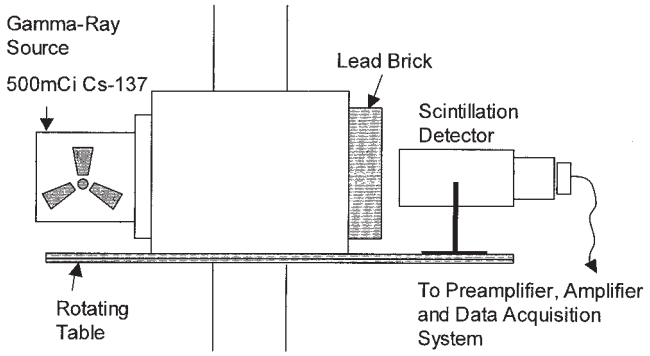

Figure 6. Gamma-ray densitometry.

Integration of Eq. 5 then gives a fourth-power dependence of granular temperature on the radius, like the thermal temperature rise in Poiseuille flow (Schlichting, 1960)

$$\theta - \theta_w = \frac{\mu_s}{\kappa_s} V_M^2 \left[1 - \left(\frac{r}{R} \right)^4 \right] \tag{7}$$

where the ratio of viscosity to conductivity is as follows

$$\frac{\mu_s}{\kappa_s} = \frac{4}{15} \quad \text{Theory (Gidaspow, 1994)} \tag{8}$$

Riser and Experimental Procedure

In collaboration with the SANDIA National Laboratory in Albuquerque, through the Fluid Dynamics Multiphase Flow Consortium (Thompson, 2002), the IIT two story riser (Miller and Gidaspow, 1992) was rebuilt with a splash plate at the top to give symmetric flow, similar to the larger unit located at SANDIA (AIChE meeting, 2001). Figure 2 shows the riser.

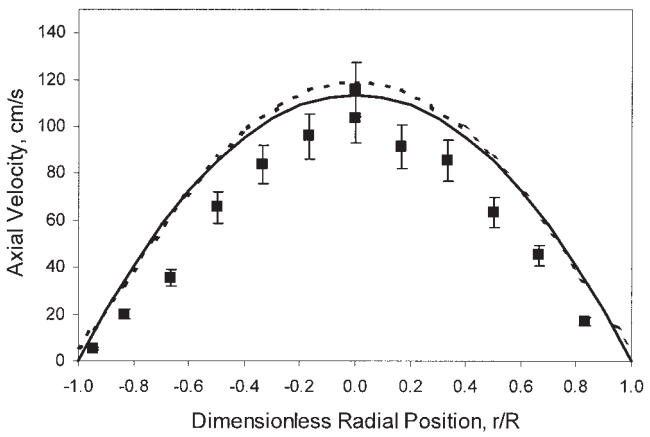

Figure 7. A comparison of the solids axial velocity distributions to the analytical solution, and the simulation.

W_s = 14.2 kg/m^2−s, U_o = 4.9 m/s, Level 4.2 m. ■ Experiment; —— Analytical solution; - - - - Numerical solution e=0.98.

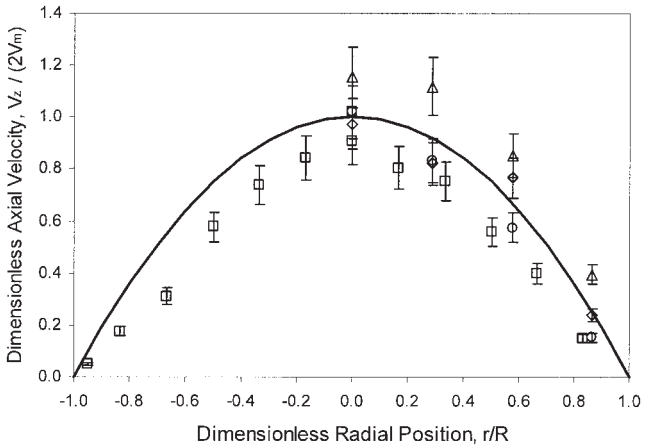

Figure 8. Universal parabolic particle velocity distribution for various solids fluxes (W_s) and inlet gas velocities (U_o).

Level 4.2 m. □ W_s = 14.2 kg/m^2-s, U_o = 4.9 m/s. ◇ W_s = 21.4 kg/m^2-s, U_o = 5.1 m/s. △W_s = 28.7 kg/m^2-s, U_o = 5.6 m/s. ○W_s = 43.9 kg/m^2-s, U_o = 6.0 m/s. —— Analytical solution.

Riser

The IIT circulating fluidized bed (CFB) was rebuilt in order to correct the nonsymmetrical behavior caused by the elbow type outlet. A splash plate replaced the nonsymmetric outlet. The splash plate was fabricated from a clear acrylic tube with a 25.4 cm OD and 61.0 cm height. The unit was originally constructed by Miller and Gidaspow (1992) at IIT. It mainly consists of a riser, a downcomer, air-solid separation cyclones, and a U-tube inlet. The riser consists of four removable sections made of acrylic tube of 7.62 cm ID, with total a height of 705 cm. Air and solids mix in the U-tube and flow through 5.1 cm ID pipe to the riser. A slide valve was used to control the solids flow to the downstream U. The outlet of the splash plate is connected to a primary cyclone, where solids and air separate by a 7.62 cm ID flexible hose. The solids discharge from the bottom of the cyclone to a 10.2 cm ID PVC pipe downcomer, which is 475 cm in length. A 10.2 cm ID butterfly valve was

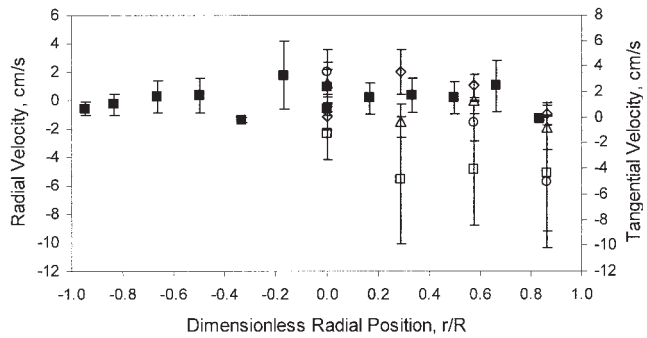

Figure 9. Radial and tangential particle-velocity distribution for various solids fluxes (W_s), and inlet gas velocities (U_o).

Level 4.2 m. □ W_s = 14.9 kg/m^2-s, U_o = 5.1 m/s (radial). ◇ W_s = 21.4 kg/m^2-s, U_o = 5.1 m/s (radial). △W_s = 28.7 kg/m^2-s, U_o = 5.6 m/s (radial). ○W_s = 43.9 kg/m^2-s, U_o = 6.0 m/s (radial). ■ W_s = 14.2 kg/m^2-s U_o = 4.9 m/s (tangential).

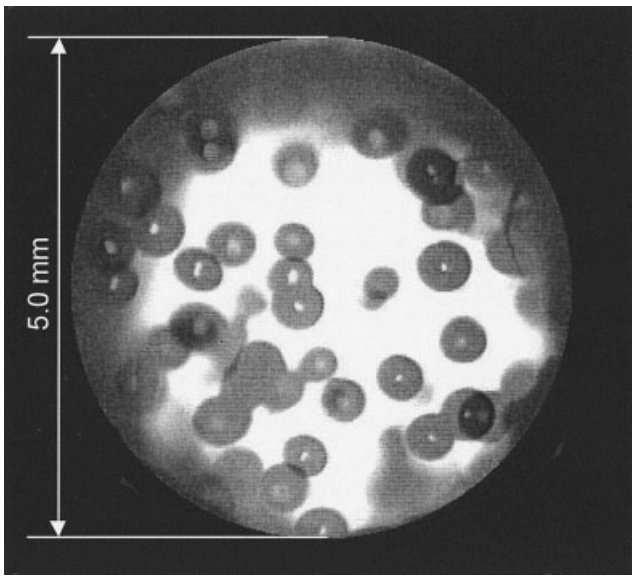

Figure 10. Particle image view through CCD camera for 530-μm glass beads.

built on the primary cyclone solids outlet pipe to measure time average solid flux by a stopwatch and ruler. The solid particles used were 530 μm glass beads with a density of 2.46 gr/cm^3.

Compressed air was introduced through three injection points in the U-tube. The slide valve at the bottom of the hopper, in the downcomer, was opened slowly until a desired solid flow rate was obtained. Glass beads from the downcomer flow to the U-tube and mix with air. The air-solid mixture flows through a 5.1 cm ID pipe to the riser. The solids flow rate was measured by closing the valve at the primary cyclone outlet pipe, and using a stopwatch and ruler. Steady-state conditions were maintained by keeping the solids level constant in the downcomer.

Particle Image Velocimetry System

Particle Image Velocimetry (PIV) described elsewhere (Gidaspow and Huilin, 1996), was used to measure the axial, radial, and tangential velocities of the particles. The system basically consists of a charge coupled device (CCD) camera, a fiber optic light, a probe, a small motor with a rotating transparency, and a personal computer with image processing software of Image-Pro Plus™. Figure 3 shows the PIV setup. In this study, we added a rotating transparency to determine the direction of the velocities by observing the order of the colors in the streak images. The camera has 10 electronic shutter settings and four modes for gain control. A metal probe of 5.8 cm length, and 0.5 cm ID was used in the experiments to obtain a radial profile of the measured values. The tip of the probe was covered with a 0.5 mm thin glass piece. The camera is connected to a personal computer, which has a micro-imaging board and micro-imaging software for data measurement and analysis. An 8.0 cm dia. colored transparent disc was used to decide the direction of particles.

A CCD camera was used to measure instantaneous particle velocities in a control volume. In order to get a good visualization of microscopic movement of particles, a fiber optic light was reflected on the field of view in the back of the riser tube. A probe passing through the annulus regime was used in the experiments to get a view in the riser. The field of view in most experiments was 0.5 cm in dia.. The various locations of the probes can be seen in Figure 4. The camera was aimed through the probe into the riser. The zoom and focus settings were set to maximum to get minimum depth of the control volume. A rotating colored transparent disc was placed in front of the light source to decide the direction of flow. The order of the colors

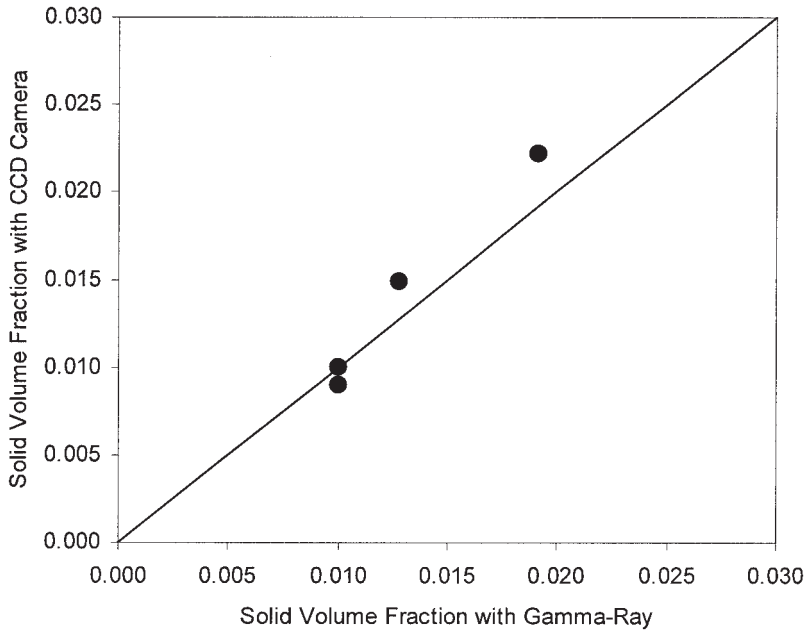

Figure 11. Average solid volume fractions measured with gamma-ray densitometry, and CCD camera.

Level 4.2 m.

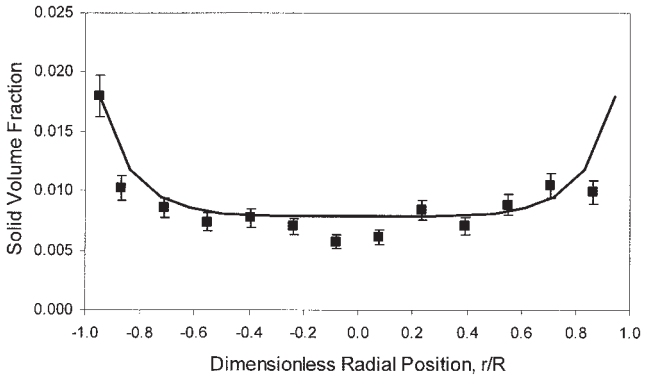

Figure 12. A comparison of solids volume fractions measured with CCD camera to the numerical solution.

Level 4.2 m. ■ Experiment (W_s = 14.2 kg/m^2-s U_o = 4.9 m/s). —— Numerical solution (e=0.98).

on the streak lines indicates the direction. Figure 5 shows typical streak lines generated on the computer screen, and their distributions. These streak lines represented the space traveled by the particles in a given time interval specified on the camera. The images were then captured and digitized by a micro-imaging board, and analyzed using Image-Pro Plus^{TM} software. Radial, tangential, and axial measurements were conducted at different locations inside the riser. The tangential and radial velocities were not measured at the same time. The velocity of a single particle was calculated as

$$c_r \text{ or } c_\theta = (L/t)\text{Cos } \alpha \tag{9}$$

$$c_z = (L/t)\text{Sin } \alpha \tag{10}$$

where L is the distance traveled or streak length, α is the angle from horizontal, t is the time elapsed by particle, which is the inverse of the shutter speed of the camera, and c_r, c_θ, c_z are the radial, tangential, and vertical velocity components, respectively.

The CCD camera was also used for estimation of solids volume fraction, and it is calculated as

$$\epsilon_s = nV_p/Ah \tag{11}$$

where ϵ_s is the solid volume fraction, n is the number of particles, V_p is the volume of a single particle, A is the view area, and h is the depth.

Gamma-ray Densitometry Experiments

The use of gamma-ray densitometries for measuring particle concentrations is a well-known technique (Gidaspow, 1994). This nonintrusive technique is based on the fact that the gas and solid phases have different absorptivities for gamma ray. The intensity of the transmitted gamma rays can be described as a linear function of the volume fractions of gas and solid phases. The Lambert-Beer's law can give the amount of radiation that is absorbed by a material

$$I = I_o\exp(-\kappa\rho l) \tag{12}$$

where I is the intensity of transmitted radiation, I_o is the intensity of incident radiation, κ is the attenuation coefficient, ρ is the density of material, and l is the path length.

The logarithmic form of the equation for gas-solid phase fluidized beds is

$$\ln(I/I_o) = A_g\epsilon_g + A_s\epsilon_s \tag{13}$$

where $A = \kappa\rho l$, ϵ_g and ϵ_s are the volume fractions of gas and solid, respectively. The relation for volume fractions is

$$\epsilon_g + \epsilon_s = 1 \tag{14}$$

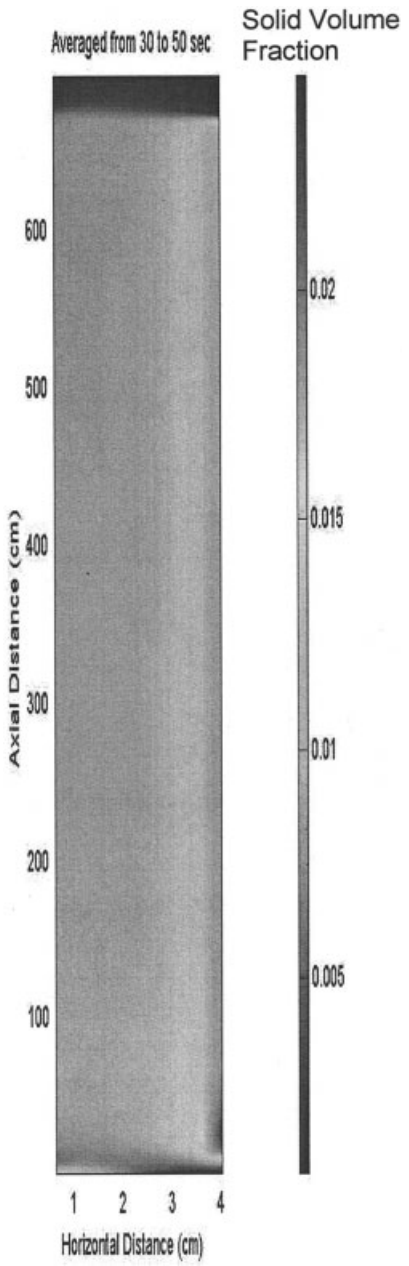

Figure 13. Simulated core-annular regimes in the riser.

W_s = 14.2 kg/m^2−s, U_o = 4.9 m/s.

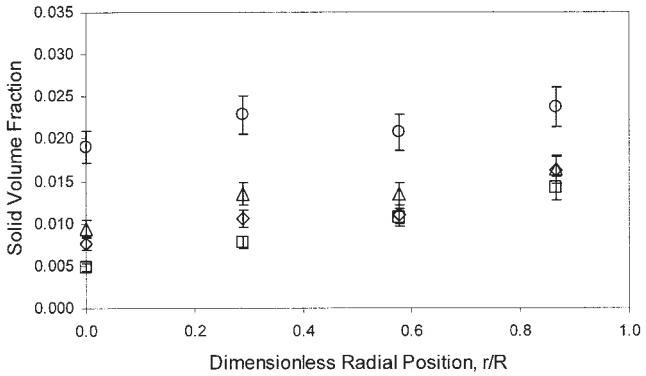

Figure 14. Solids volume fraction distributions at higher fluxes.

Level 4.2 m. □ W_s = 14.9 kg/m^2-s, U_o = 5.1 m/s. ◇ W_s = 21.4 kg/m^2-s, U_o = 5.1 m/s. △W_s = 28.7 kg/m^2-s, U_o = 5.6 m/s. ○W_s = 43.9 kg/m^2-s, U_o = 6.0 m/s.

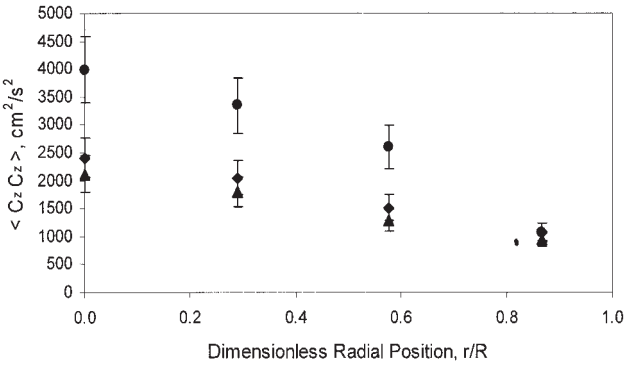

Figure 16. Normal stresses per unit bulk density in the direction of flow for denser flow.

Level 4.2 m. ♦ W_s = 21.4 kg/m^2-s, U_o = 5.1 m/s. ▲ W_s = 28.7 kg/m^2-s, U_o = 5.6 m/s. ●W_s = 43.9 kg/m^2-s, U_o = 6.0 m/s.

The coefficients in Eq. 13 were calculated by measuring the radiation intensities at known solid volume fractions as described earlier (Seo and Gidaspow, 1987; Gidaspow et al., 1983).

Time and area-averaged solid volume fractions at a specific location were obtained by converting the voltage readings from the data acquisition system using a calibration curve. Radiation counts were converted to voltage by a rate meter. Data was recorded by the data acquisition system at least for 1 min long, with a 0.03 s sampling time at a specific location.

The gamma-ray source is a 500 mCi-Cs-137 source, having a single gamma ray of 667 keV, and a half-life of 30 years (see Figure 6). The Cs-137 source was sealed in a welded stainless steel capsule. The source holder was welded, filled with lead, and provided with a shutter to turn off the source. The transmitted beam intensity was measured by using a NaI(Ti) crystal scintillation detector (EG&G Model 905), which was connected to photo multiplier base (EG&G Model 266). The signals from the photo multiplier were passed through a preamplifier, an amplifier, and a single-channel analyzer, a rate meter, and a data acquisition system. The rate meter has a selector and a 0-100-mV scale range. The beam from the source was collimated through a 1.27 cm hole on 3.8 cm thick lead plate.

Data Acquisition System

Signals from the gamma ray come to data acquisition system. The data acquisition system consists of a software program, hardware devices, and a 500 MHz Pentium™ III personal computer. The software is Lab-View 5.0 program. The hardware parts are DAQ board, SC-2050 Adapter (National Instruments) and Voltage Input Module (Model 5B41-01, Analog Devices), which accepts -1V to 1V input signals, and provides -5V to 5V output, for data measurement and analysis.

Experimental Results

Time averaged hydrodynamic particle velocities

Instantaneous radial particle velocity distributions of 530 μm glass beads were measured using our improved CCD camera technique by inserting a probe into the riser. Radial distribution of time-averaged axial, radial, and tangential solid-

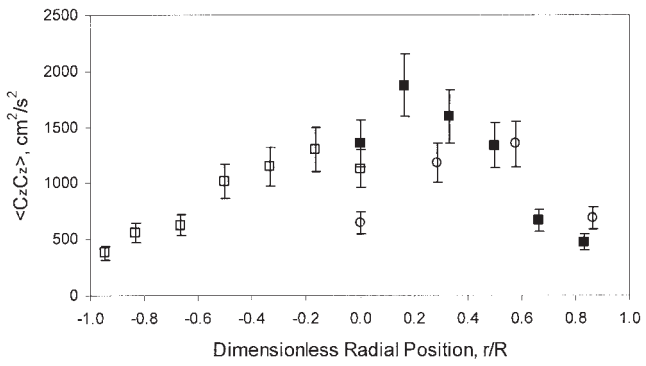

Figure 15. Normal stresses per unit bulk density in the direction of flow for two similar conditions for dilute flow.

Level 4.2 m. □ W_s = 14.2 kg/m^2-s, U_o = 4.9 m/s (measured from left). ■W_s = 14.2 kg/m^2-s, U_o = 4.9 m/s (measured from right). ○W_s = 14.9 kg/m^2-s, U_o = 5.1 m/s.

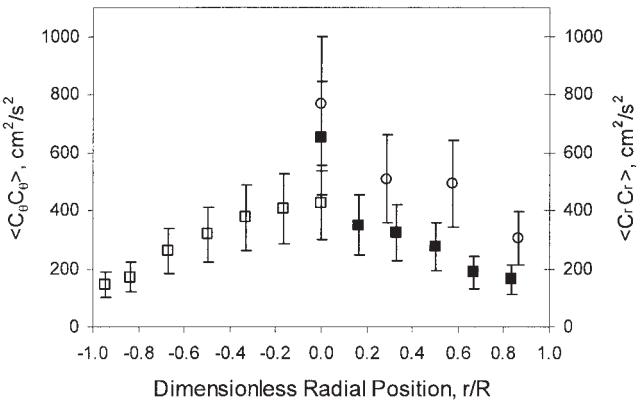

Figure 17. Radial and tangential normal stresses per unit bulk density.

Level 4.2 m. □ $\langle C_\theta C_\theta \rangle$ W_s = 14.2 kg/m^2-s, U_o = 4.9 m/s (measured from left). ■ $\langle C_\theta C_\theta \rangle$ W_s = 14.2 kg/m^2-s, U_o = 4.9 m/s (measured from right). ○ $\langle C_r C_r \rangle$ W_s = 14.9 kg/m^2-s, U_o = 5.1 m/s.

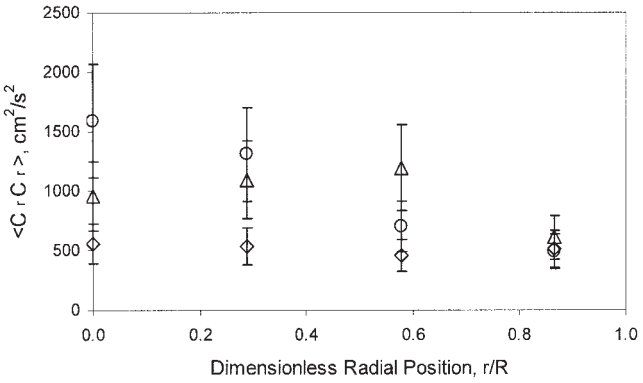

Figure 18. Radial normal stresses per unit bulk density for denser flow.

Level 4.2 m. ◇ W_s = 21.4 kg/m^2-s, U_o = 5.1 m/s. △W_s = 28.7 kg/m^2-s, U_o = 5.6 m/s. ○W_s = 43.9 kg/m^2-s, U_o = 6.0 m/s.

phase velocities, were obtained at heights of 4.2 m and 5.0 m of the riser inlet. Experiments were carried out at five different flow conditions at a height of 4.2 m, and at one-flow condition at a height of 5.0 m.

Radial distributions of axial, tangential, and radial particle velocities are shown in Figures 7 to 9 for a range of solid fluxes and gas velocities obtained in the IIT riser in the circulating fluidized-bed regime. At much higher solid fluxes and much lower gas velocities, we reached the limiting carrying capacity of the riser called choked flow.

Figure 7 shows the axial velocity profile measured with a probe inserted from both sides. The error bars were estimated from duplicate measurements. The experimental errors are larger near the center, due to a possible disturbance by the probe. The analytical solution was determined by computing the mean velocity V_{sM} in Eq. 3, by use of Eq. 4.

Here

$$V_{sM} = \frac{1.42}{0.01 \times 2.5} = 56.8 \text{ cm/s}$$

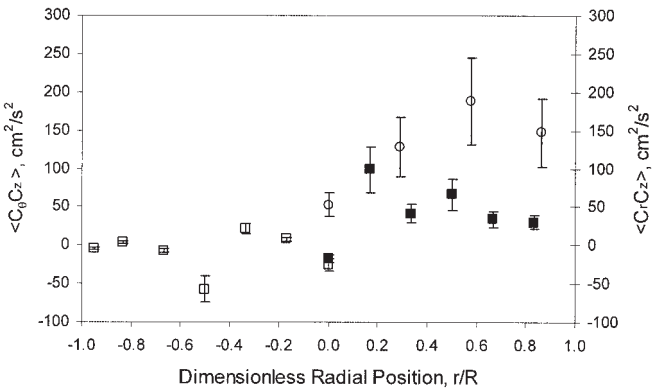

Figure 19. Radial and tangential shear stresses per unit bulk density for dilute flow.

Level 4.2 m. □ $\langle C_\theta C_z \rangle$ W_s = 14.2 kg/m^2-s, U_o = 4.9 m/s (measured from left). ■ $\langle C_\theta C_z \rangle$ W_s = 14.2 kg/m^2-s, U_o = 4.9 m/s (measured from right). ○ $\langle C_r C_z \rangle$ W_s = 14.9 kg/m^2-s, U_o = 5.1 m/s.

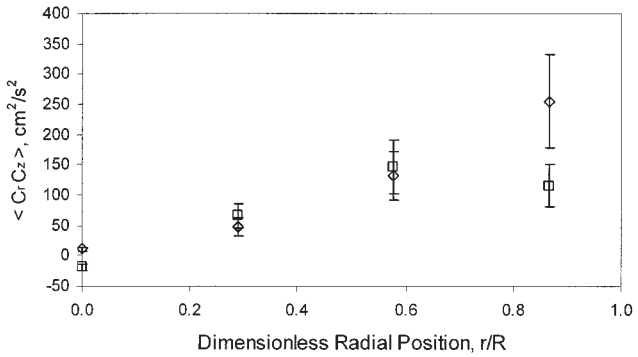

Figure 20. Radial shear stresses per unit bulk density for higher flux.

Level 4.2 m. ◇ W_s = 21.4 kg/m^2-s, U_o = 5.1 m/s. □W_s = 43.9 kg/m^2-s, U_o = 6.0 m/s

The lack of perfect agreement between the experiment and analytical solution is due to neglect of the thin annular region. The small difference between the simulation and the experiment is probably due to the fact that the computer code did not predict the small-scale turbulence observed in the experiment.

Figure 8 shows the comparison of all the axial velocity distributions determined in this study to the parabolic velocity distribution. The data for all but the flux shown in Figure 7, were obtained from one side only. Figure 9 summarizes the radial and tangential velocities. They are much smaller than the axial velocities shown in Figure 7 and 8. Hence, the error bars in Figure 9 are larger than those in Figure 8. Since the radial and tangential velocities were small compared to the axial velocity, the flow is developed.

Solid Phase Volume Fraction Distributions

Solid volume fractions of 530 μm glass beads were estimated by using the CCD camera technique. Figure 10 shows a typical view of the particles through the probe at the highest shutter speed. At lower shutter speed, streaks are obtained. Instantaneous particle concentration can be obtained by count-

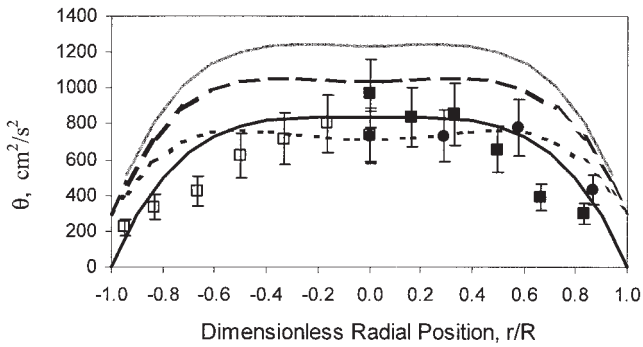

Figure 21. A comparison of granular temperature to an analytical solution obtained from kinetic theory and to numerical solutions.

Level 4.2 m. □ W_s = 14.2 kg/m^2-s, U_o = 4.9 m/s (measured from left). ■W_s = 14.2 kg/m^2-s, U_o = 4.9 m/s (measured from right). ●W_s = 14.9 kg/m^2-s, U_o = 5.1 m/s. —— Analytical solution; —— numerical solution e = 0.98; – – numerical solution e = 0.95; - - - - numerical solution e = 0.89.

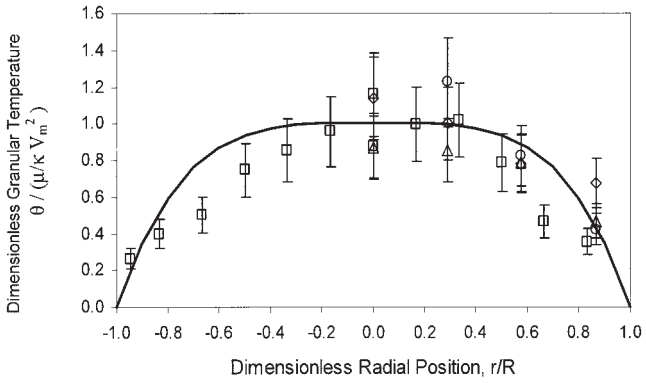

Figure 22. Comparison of dimensionless granular temperature to dimensionless analytical solution.

Level 4.2 m. □ W_s = 14.2 kg/m^2-s, U_o = 4.9 m/s. ◇ W_s = 21.4 kg/m^2-s, U_o = 5.1 m/s. △W_s = 28.7 kg/m^2-s, U_o = 5.6 m/s. ○W_s = 43.9 kg/m^2-s, U_o = 6.0 m/s. — Dimensionless Analytical Solution.

ing the number of streaks per unit volume. The depth was estimated by moving the camera backward and forward until the object goes out of focus. A typical depth is 7 mm. Area and time-averaged solid volume fractions were also acquired by using gamma-ray densitometry. As it can be seen in Figure 11, there is fairly good agreement between solid volumes fractions measured by the two methods.

Figure 12 shows a comparison of the measured solid-volume fractions to the numerical simulation. The solid-volume fractions in Figure 12 at the left wall were determined without using the probe. The agreement between the simulation and the experiment is within the experimental error. Figure 13 shows the fully developed core annular structure. Due to the inlet geometry in the IIT riser, the densest portion is not at the very bottom of the riser. This phenomenon was already observed in the simulation of Neri and Gidaspow (2000). The solid volume-fraction distributions for the higher fluxes are shown in Figure 14.

Solid Phase Normal and Shear Stresses

Variances of fluctuating velocity in axial, radial, and tangential direction were calculated from instantaneous particle velocity measurements. The fluctuating velocity, also called as

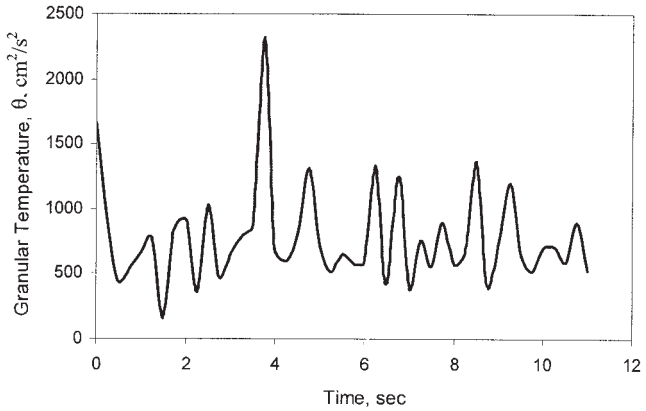

Figure 23. Variation of granular temperature with time.

Level 4.2 m. W_s = 14.9 kg/m^2-s, U_o = 5.1 m/s. r/R = 0.58.

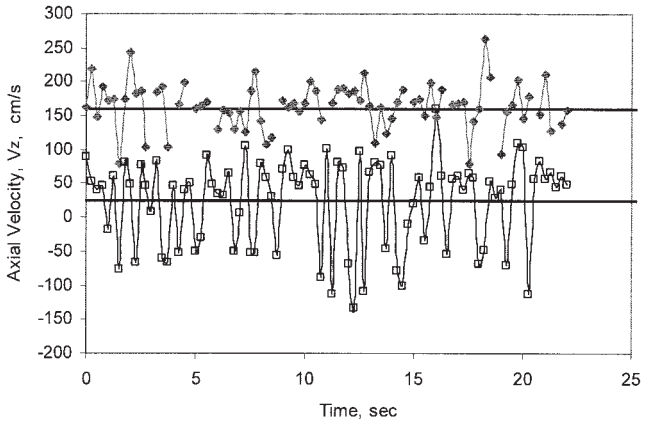

Figure 24. Typical time series of axial velocity.

W_s = 43.9 kg/m^2−s, U_o = 6.0 m/s Level 4.2 m. ◆ r/R = 0/0. □ r/R = 0.87.

peculiar velocity, is defined as instantaneous particle velocity minus hydrodynamic velocity

$$\langle C_i C_j \rangle(t, \mathbf{x}) = \frac{1}{N} \sum_{k=1}^{N} (c_{ik} - v_i)(c_{jk} - v_j) \tag{15}$$

The hydrodynamic velocity v_i is computed as the average value in each figure, as

$$v_i(t, \mathbf{x}) = \frac{1}{N} \sum_{k=1}^{N} c_{ik}(t, \mathbf{x}) \tag{16}$$

$$\overline{\langle C_i C_j \rangle}(\mathbf{x}) = \frac{1}{T} \int_{t}^{t+T} \langle C_i C_j \rangle(t, \mathbf{x}) dt \tag{17}$$

where N is the number of particles per unit volume; c_{ik} is the instantaneous particle velocity in the ith-direction for the kth streak

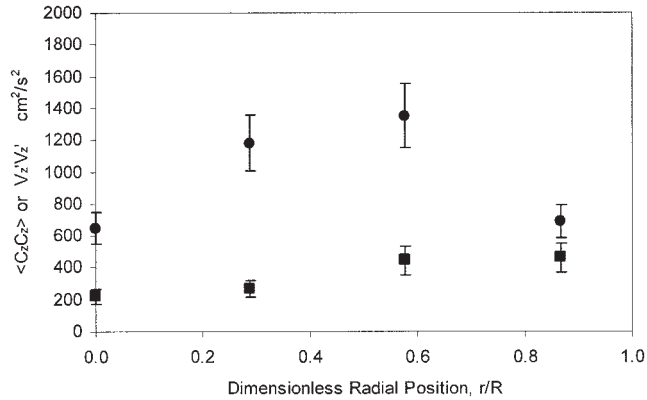

Figure 25. Normal stress per unit bulk density and normal Reynolds stress per unit bulk density for dilute flow.

W_s = 14.9 kg/m^2−s, U_o = 5.1 m/s Level 4.2 m. ■ $V_z'V_z'$; ● $\langle C_z C_z \rangle$

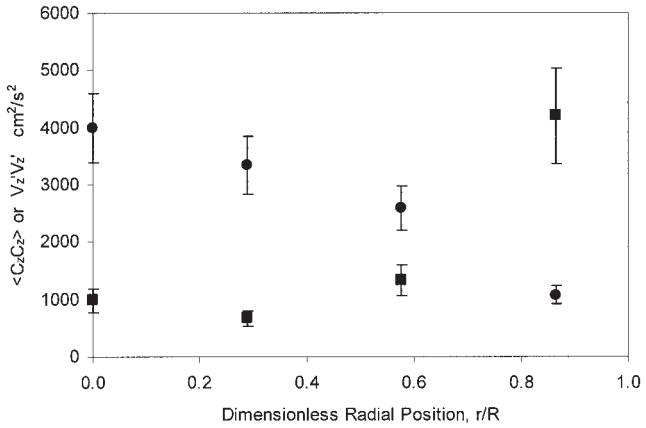

Figure 26. Normal stress per unit bulk density and normal Reynolds stress per unit bulk density for dense flow.

W_s = 43.9 kg/m^2−s, U_o = 6.0 m/s. Level 4.2 m. ■ V_z'V_z'; ● $\langle C_zC_z\rangle$.

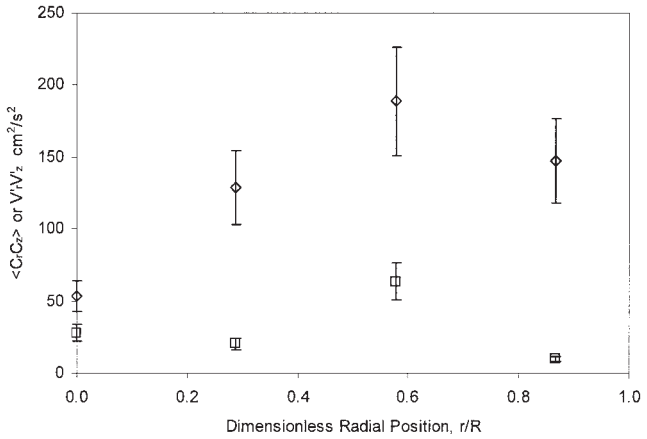

Figure 28. Shear particle and Reynolds stresses per unit bulk density for dilute flux.

W_s = 14.9 kg/m^2−s, U_o = 5.1 m/s. Level 4.2 m. ◇ $\langle C_zC_z\rangle$; □V_z'V_z'.

in a single frame; v_i is the instantaneous hydrodynamic velocity in the ith-direction; *i is r*, θ, *z;* and T is the time interval.

Figures 15 to 18 show the time-average values of the normal stresses per unit bulk density, $\epsilon_s\rho_s$, $\langle C_rC_r\rangle$,, $\langle C_\theta C_\theta\rangle$ and $\langle C_zC_z\rangle$ as a function of the radial position for various solid fluxes and gas flow rates. The variances of fluctuating velocity in the direction of flow $\langle C_zC_z\rangle$ are approximately 2 to 3 times higher than those in the radial and tangential directions. This is due to the high gradient of axial velocity. In developed flow, the radial, and tangential velocities are quite small and, hence, their gradients are also small. However, the magnitudes of variances in radial and tangential directions are close to each other as it can be seen in Figure 17. Similar to the flow of FCC particles (Gidaspow and Huilin, 1996), isotropy does not hold.

Time averages of $\langle C_rC_r\rangle$ and $\langle C_\theta C_\theta\rangle$ is higher at the center and lower at the wall of the riser. The trend for $\langle C_zC_z\rangle$ is similar to that for the variances of fluctuating velocity in radial and tangential directions, except for the more dilute case. In this case, $\langle C_zC_z\rangle$ has a maximum somewhere between the center and the wall (See Figure 15). Close to the center, the normal velocity fluctuations increase as the solid fluxes increase. However, the fluctuation values in radial, tangential, and axial directions are getting closer near the wall. Isotropy can be a fair assumption in this region for the given flow conditions.

The time-average values of the shear stresses per unit bulk density, $\langle C_\theta C_z\rangle$ and $\langle C_rC_z\rangle$ as a function of the radial position for various solid flux and superficial gas velocity, are plotted in Figures 19 and 20. The $\langle C_rC_z\rangle$ values are close to zero at the center and monotonically increase toward to the wall. This behavior is similar to that for gas flow. Near the wall there is generally a decrease as shown Figures 19 and 20. Shear stresses allow us to estimate the restitution coefficients for the particles (Tartan, 2003).

Granular Temperature

The granular temperature is calculated by using the following definition

$$\theta(t, \mathbf{x}) \equiv \frac{1}{3}\langle C_rC_r\rangle + \frac{1}{3}\langle C_\theta C_\theta\rangle + \frac{1}{3}\langle C_zC_z\rangle \qquad (18)$$

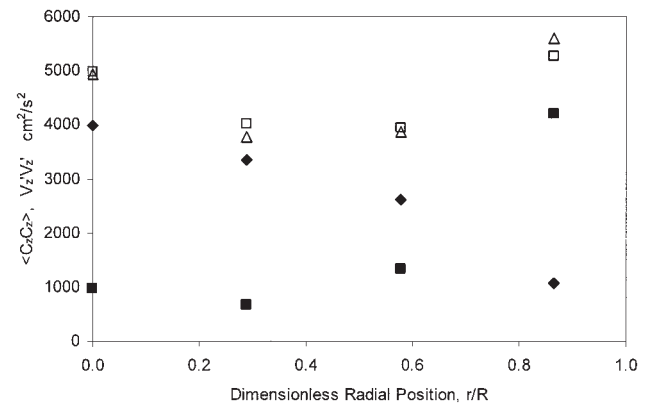

Figure 27. Total normal stresses per unit bulk density.

■V_z'V_z'; ◆$\langle C_zC_z\rangle$ (instantaneous); △$\langle C_zC_z\rangle$ (overall); □$\langle C_zC_z\rangle$ + V_z'V_z'.

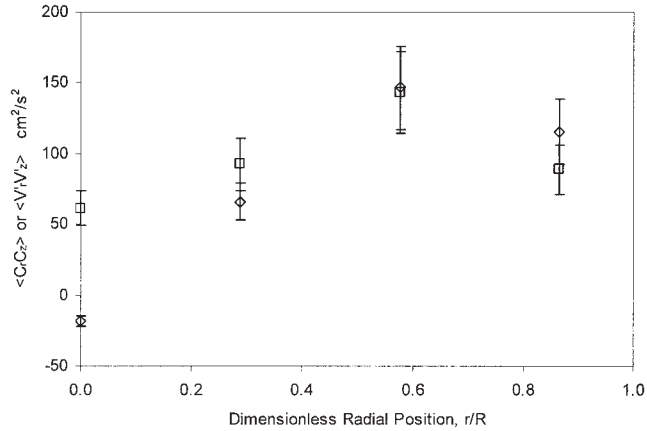

Figure 29. Shear particle and Reynolds stresses per unit bulk density for dense flux.

W_s = 43.9 kg/m^2−s, U_o = 6.0 m/s Level 4.2 m. ◇ $\langle C_zC_z\rangle$; □V_z'V_z'.

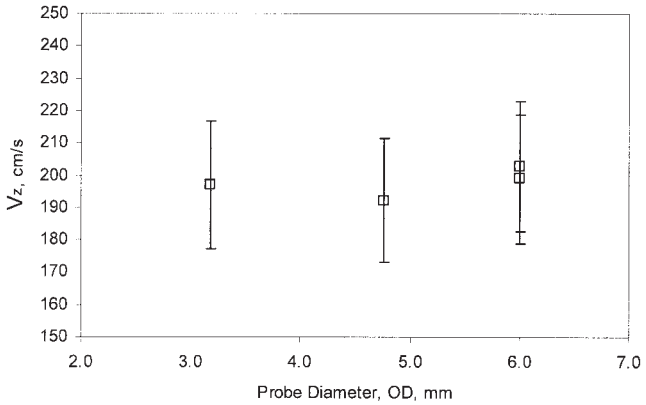

Figure 30. Effect of probe diameter on velocity measurements.

W_s = 44.9 kg/m^2−s, U_o = 6.4 m/s. Level 4.2 m.

By assuming that the fluctuations are equal in the radial and the tangential directions, the definition can further be simplified to

$$\theta(t, \mathbf{x}) \cong \frac{2}{3}\langle C_r C_r \rangle + \frac{1}{3}\langle C_z C_z \rangle \tag{19}$$

This assumption was experimentally verified in this study, as seen in Figure 17. Figure 21 shows a comparison of the experimentally measured granular temperature to the analytical solution, and to the simulations for several values of the restitution coefficients. The restitution coefficient of 0.98 is obtained from the ratio of shear stress to granular temperature (Eq. 20 in Gidaspow's (2003) review). This equation can be obtained by equating production of granular temperature due to the shear gradient in the direction of flow, to dissipation due to inelastic collisions. The biggest inaccuracy in this equation is the neglect of dissipation due to the drag between the particles and the fluid. The effect of the neglect of conduction in the core introduces a smaller error than the neglect of the drag. The effect of the drag can be roughly estimated from Gidaspow's (2003) Eq. 23. This equation includes the dissipation due to drag using Stokes flow, and dissipation due to collisions. It has to be corrected for the inapplicability of Stokes flow. The result of such an estimate is a restitution coefficient much lower than 0.98. This rough analysis justifies the observed match of the data to the numerical solution with the restitution coefficient of 0.89. However, the data empirically matches the analytical solution with zero wall temperature. This solution is, of course, not valid in the annular region. The computer code did not predict well the granular temperature in the annular region. This lack of agreement was probably due to the assumption of axial symmetry and isotropy in the kinetic theory model.

Figure 22 shows that all the measured granular temperatures in the core of the riser can be approximated by the analytical solution, with zero wall granular temperature within experimental error. Figure 23 shows the typical behavior of granular temperature with time.

Reynolds Stresses

Variation of axial velocity as shown in Figure 24 permits the determination of Reynolds stresses per unit bulk density. Equations given below are similar but not identical to those given for particle stresses

$$\bar{v}_i(\mathbf{x}) = \frac{1}{T}\int_t^{t+T} v_i(t, \mathbf{x})dt \tag{20}$$

$$v_i' v_j'(t, \mathbf{x}) = (v_i - \bar{v}_i)(v_j - \bar{v}_j) \tag{21}$$

$$\overline{v_i' v_j'}(\mathbf{x}) = \frac{1}{T}\int_t^{t+T} v_i' v_j'(t, \mathbf{x})\, dt \tag{22}$$

where v_i is the hydrodynamic velocity in ith-direction; i or j is r, θ, z; and T is the time interval.

Shear and normal Reynolds stresses per unit bulk density were computed for different fluxes and velocities analogous to particle shear and normal stresses (Tartan, 2003; Tartan and Gidaspow, 2002).

Comparison of normal stress per unit bulk density to the normal Reynolds stress per unit bulk density for dilute flow is shown in Figure 25. Except near the wall, normal Reynolds stress per unit bulk density is substantially below the particle stress per unit bulk density. At the highest flux, the normal Reynolds stress per unit bulk density becomes much higher than the particle stress per unit bulk density (see Figure 26). This can be visually seen by observing the large fluctuations at the wall. Figure 24 shows this effect quantitatively. The large particle stresses per unit bulk density at the center of the riser show that mixing occurs due to particle oscillations, similarly, molecular type diffusion for fluids.

Tsuji et al. (1984) have a measured particle turbulent intensity for 500 micron plastic particles for very dilute conditions. Their turbulent intensity for air shows a similar behavior to that of particles depicted in Figure 25. The turbulent intensity at the center from Figure 25 is 0.128 vs. that of Tsuji et al. (1984) of 0.052 for a more dilute flow. Since the turbulence increases with particle concentration, our data and trend are consistent with that of Tsuji et al. (1984).

The Reynolds stresses per unit bulk density, and the particle stresses per unit bulk density added up to total stresses for the

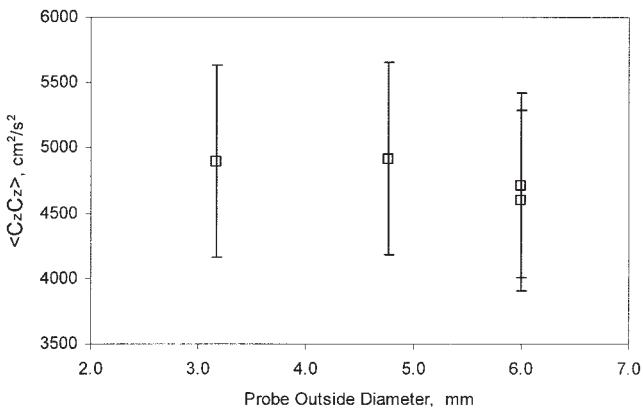

Figure 31. Effect of probe diameter on stress measurements.

W_s = 44.9 kg/m^2−s, U_o = 6.4 m/s. Level 4.2 m.

Table 5. Estimate of Solids Viscosities

W_s (kg/m^2 − s)	r/R	μ_s^{laminar} (mPa · s)	$\mu_s^{\text{turbulent}}$ (mPa · s)	$\mu_s^{\text{kin theory}}$ (mPa · s)	μ^{total} (mPa · s)
	0.29	12	2	26	39
	0.58	12	4	26	26
14.9	0.87	9	1	19	12
	0.29	7	3	30	36
	0.58	9	1	27	33
21.4	0.87	18	3	24	23
	0.29	16	22	40	34
	0.58	16	16	33	37
43.9	0.87	10	7	24	38

$$\mu_s^{\text{laminar}} = \frac{\epsilon_s \rho_s \langle C_r C_z \rangle}{dv_{sz}/dr}$$

$$\mu_s^{\text{turbulent}} = \frac{\epsilon_s \rho_s \overline{v'_{sr} v'_{sz}}}{dv_{sz}/dr}$$

$$\mu_s^{\text{kin theory}} = \frac{5\sqrt{\pi}\rho_s d_p \sqrt{\theta}}{48(1+e)g_o}\left[1+\frac{4}{5}(1+e)g_o\epsilon_s\right]^2 + \frac{4}{5}\epsilon_s^2\rho_s d_p(1+e)g_o\sqrt{\frac{\theta}{\pi}}$$

$$\mu^{\text{total}} = \frac{-\frac{dP}{dz}\frac{1}{2}r^2 - \int_0^r \epsilon_s \rho_s g r dr}{-r\left.\frac{dv_{sz}}{dr}\right|_r}$$

system. Total stresses per unit bulk density can be obtained either by adding particle stresses per unit bulk density and Reynolds stresses per unit bulk density, or by obtaining the total stresses per unit bulk density by considering all the frames together, independent of time. Figure 27 shows that the computation of the total stresses per unit bulk density by the two methods gives similar results. The small difference is due to use of insufficient particles per frame. A similar analysis was performed by Mudde et al. (1997) for gas-liquid flow.

Figure 28 shows a comparison of the shear particle and Reynolds stresses per unit bulk density for dilute flow. The Reynolds stresses per unit bulk density are smaller than the particle stresses per unit bulk density. However, for dense flow, Figure 29 shows that the stresses per unit bulk density are close to each other. This observation agrees with the analyses of Dasgupta et al. (1998).

Effect of probe

Measurements were repeated using three different probes at the highest flux. Figure 30 shows the duplicate particle velocity in the center of the tube for 6.0 mm OD, and the velocities for two smaller probes. The corresponding normal stresses are shown in Figure 31. The effect of the probe is small. It is, however, impossible to use the smaller probes for a frame-by-frame analysis. The stress shown in Figure 31 is a sum of the Reynolds stress per unit bulk density, and particle stress per unit bulk density.

Laminar and Turbulent Viscosities

Table 5 shows laminar and turbulent viscosities computed from the shear and Reynolds stresses using the equations shown in the table. Table 5 also shows the kinetic theory viscosity computed from the granular temperature measurements, and the total viscosity obtained from pressure drop minus the weight of the bed measurements. The laminar shear viscosity is higher than the turbulent shear viscosity for low solids fluxes. At the highest solids flux they are of the same order of magnitude. The viscosity obtained from the kinetic theory is close to the viscosity obtained from the mixture equation. The same result was obtained by Gidaspow and Huilin (1996) for flow of FCC particles. These viscosities are about double the shear viscosities. We believe these differences are due to the strong anisotropy of flow.

Figure 32 shows a comparison of the kinetic theory, and the total viscosity to that obtained from the simulation for the low-flux flow. In general, the viscosities are nearly constant in the core of the riser. This is due to the fact that the granular temperature is nearly flat in the core, and the viscosity is almost independent of the solids volume fraction in the range of riser measurements.

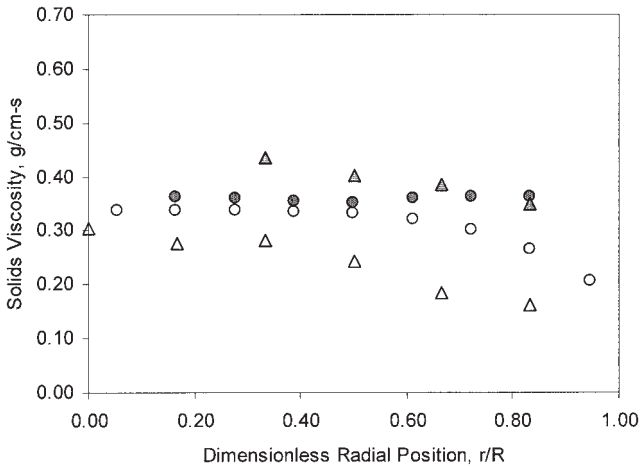

Figure 32. Radial variation of solids viscosity.

W_s = 14.2 kg/m^2−s, U_o = 4.9 m/s. Level 4.2 m. ○ Kin. theory (simulation, e=0.98). △ Kin. theory (experiment) ● Total Stress (Simulation, e=0.98). ▲ Total stress (experiment).

Conclusions

(1) Time-averaged solid velocity profiles in the developed region of a riser with a splash plate can be described by a laminar type parabolic velocity distribution in the range measured. All the data can be fitted to the least square equation $V_z/2V_M = 0.96\ [1-(r/R)^2]$ with a coefficient of determination (R^2) of 0.85.

(2) Granular temperature profiles for developed flow can be described by a simple expression derived from kinetic theory assuming the particles to be completely elastic, similar to the thermal temperature distribution in Poiseuille flow with viscous heat generation. All the data can be fitted to the least square equation, $\theta/(\mu/\kappa\ V_M^2) = 0.96\ [1-(r/R)^4]$, where the ratio of viscosity to conductivity was equal to the theoretical value of 4/15, and V_m was the experimentally determined value of the averaged-particle velocity. The coefficient of determination (R^2) was 0.65.

(3) Particle shear and normal stresses have been measured in the developed region of the riser. The normal stresses in the direction of flow are much larger than the tangential and radial normal stresses. Similar anisotropy was observed for flow of FCC particles in the riser (Gidaspow and Huilin, 1996).

(4) A numerical solution of the transient 2-D isotropic kinetic theory model, as given by Neri and Gidaspow (2000), shows that the flow is in the developed laminar type core-annular regime, and that the approximations made in the analytical solution are reasonable.

(5) Reynolds stresses were obtained by time-averaging hydrodynamic velocities. In the core, the Reynolds stresses are much smaller than the velocity averaged shear stresses. Near the wall, the Reynolds stresses are large, as visually observed. This means that the mixing in a riser is due to particle oscillations, like the molecular diffusivity for fluids. The total stresses can be obtained as a sum of particle stresses and Reynolds stresses, similarly to that done by Mudde et al. (1997) for gas liquid flow.

Laminar type shear viscosities were generally smaller than the turbulent shear viscosities. The viscosities computed from the kinetic theory were close to those computed from pressure, the drop minus the weight of bed measurements. Complete understanding of riser flow requires measurements of gas velocities, and the development of an anisotropic kinetic theory.

(6) Measurements were done with probes of three different diameters. The probe did not significantly affect the measurements of velocity and stresses.

Acknowledgment

This study is partially supported by the National Science Foundation grant CTS 0086250.

Notation

c = instantaneous particle velocity
C = peculiar velocity, c-v
d_p = particle diameter
e = coefficient of restitution
g = gravitational acceleration
g_o = radial distribution function
I = radiation intensity
n = number of particles
P = pressure
r = radial coordinate
R = pipe radius
t = time
T = time interval
U_o = superficial gas velocity
v = hydrodynamic velocity
V_M = mean particle velocity, averaged over pipe radius
W_s = solid fluxes

Greek Letters

β = drag coefficient between phases
ϵ_k = volume fraction of phase "k"
τ = stress
μ = shear viscosity
κ = granular conductivity
ρ = density
θ = granular temperature

Literature Cited

Anderson, K., S. Sundaresan, and R. Jackson, "Instabilities and the Formation of Bubbles in Fluidized Beds," *J. Fluid Mech*., **303**, 327 (1995).

Arena, V., K. Cammarato, K. Marzocchella, and L. Massinilla, "Solids Flow Structures in a Two Dimensional Riser of a Circulating Fluidized Bed," *J. Chem. Eng. of Japan*, **22**, 236 (1989).

Avidan, A. A., M. Edwards, and H. Owen, "Fluid-Catalytic Cracking-Past and Future Challenge," *Chem. Eng.*, **6**, 1 (1990).

Azzi, M., P. Turfier, J. R. Bernard, and L. Garnero, "Mapping Solid Concentration in a Circulating Fluid Bed Using Gammametry," *Powder Tech*., **67**, 27 (1991).

Bader, R. J., Findlay, and T. M. Knowlton, "Gas/Solid Flow Patterns in a 30.5-Cm-Diameter Circulating Fluidized Bed," *Circulating Fluidized Bed Technology II,* P. Basu and J. F. Large, eds., Pergamon Press, Oxford, U.K., 123 (1988).

Benyahia S., H. Arastoopour, and T. M. Knowlton, "Prediction of Solids and Gas Flow Behavior in a Riser Using a Computational Multiphase Flow Approach," *Proc. 9 th Eng. Found. Conf. Fluidization*, Durango, CO, Engineering Foundation, New York (1998).

Berruti, F., J. Chaouki, L. Godfroy, T. S. Pugsley, and G. S. Patience, "Hydrodynamics of Circulating Fluidized Bed Risers: A Review," *Canadian J. Chem. Eng*., **73**, 579 (1995).

Cao, J., and G. Ahmadi, "Gas Particle Two Phase Turbulent Flow in a Vertical Duct," *Int. J. Multiphase Flow*, **21**, 1203 (1995).

Crowe, C. T., T. R. Troutt, and J. N. Chung, "Numerical Models for Two-Phase Turbulent Flows," *Annu. Rev. Fluid Mech*., **28**, 11 (1996).

Crowe, C. T., "Multiphase Flow Models for Industrial Applications," *AIChE Annual Meeting Preprints*, Advanced Technologies for Particle Processing, Vol. II, Miami Beach, FL, 503 (1998).

Crowe, C., "Carrier Phase Turbulence in Multiphase Flows," *Multiphase Fluid Dynamics Research Consortium, Semi- Annual Meeting and Review*, Albuquerque, NM (Apr. 12–14, 2000).

Dasgupta, S., R. Jackson, and S. Sundaresan, "Turbulent Gas-Particle Flow in Vertical Risers," AIChE J., 40, 215 (1994).

Dasgupta, S., R. Jackson, and S. Sundaresan, "Gas-Particle Flow in Vertical Pipes with High Mass Loading of Particles," Powder Tech., 96, 6 (1998).

Dudukovic, M., "Use of Radioactive Particle Tracking in Mapping the Solids Flow Field in Risers," Multiphase Fluid Dynamics Research Consortium, Semi- Annual Meeting and Review, Albuquerque, NM (Apr. 12–14, 2000).

Enwald, H., E. Peirano, and A. -E. Almstedt, "Eulerian Two-Phase Flow Theory Applied to fluidization," Annual Reviews in Multiphase Flow, Int. J. of Multiphase Flows, 22, 21 (1996).

Galtier, P. A., R. J. Pontier, and T. E. Patereaux, "Near Full-Scale Cold Flow Model for the R2R Catalytic Cracking Process," Fluidization VI, J. R. Grace, L. W. Shemilt, and M. A. Bergougnou, eds., Engineering Foundation, New York, pp. 17–24 (1989).

Gidaspow, D., Multiphase Flow and Fluidization: Continuum and Kinetic Theory Descriptions, Academic Press, San Diego (1994).

Gidaspow, D., "Computation/Measurement of Turbulence & Structure in Risers & Bubbling Beds," Multiphase Fluid Dynamics Research Consortium (MFDRC) Semi-Annual Meeting and Review, Albuquerque, NM (Apr. 12–14, 2000).

Gidaspow, D., "Hydrodynamics of Fluidization Using Kinetic Theory: An Emerging Paradigm?," *Recent Res. Devel. Chem. Eng*., **5**, 53, Transworld Research Network, Kerach, India (2003).
Gidaspow, D., and L. Huilin, "Collisional Viscosity of FCC Particles in a CFB," *AlChE J*., **42**, 2503 (1996).
Gidaspow, D. and L. Huilin, "Equation of State and Radial Distribution Functions of FCC Particles in a CFB," *AlChE J*., **44**, 279 (1998).
Gidaspow, D., Lin, C., and Y. Seo, "Fluidization in Two-Dimensional Beds with a Jet. 1. Experimental Porosity," *Ind. Eng. Chem. Fund*., **22,** 187 (1983).
Gidaspow, D., Y. P. Tsuo, and K. M. Luo, "Computed and Experimental Cluster Formation and Velocity Profiles in Circulating Fluidized Beds," *Fluidization VI*, J. R. Grace, L. W. Shemilt, and M. A. Bergougnou, eds., Engineering Foundation, New York, p. 81 (1989).
Gidaspow, D., Y. P. Tsuo, and J. Ding, "Hydrodynamics of Circulating and Bubbling Fluidized Beds," *Fluids Engineering: Korea-U.S. Progress*, J. H. Kim, J. M. Hyun, and C. O. Lee, eds., Hemisphere Publishing Corporation, New York, p. 485 (1991).
Grace, J. R., J. Zhao, R. Wu, R. Seniorg R. Legros, C. M. H. Brereton, and C. J. Lim, "Spatial Variations Inside a Pilot Scale CFB Unit," 10-1 to 10-21, *Proc. Workshop on Issues in Circulating Fluidized Bed Combustors*, Electric Power Research Institute, EPRI GS- 6747 (Feb. 1990).
Hjertager, B. H., V. Mathiesen, and T. Solberg, "Computational Analysis of Some Fluidized Systems," *AIChE Symp. Series*, Vol. II, Miami Beach,262, Nov. 15–20, (1998).
Hrenya, C. M., and J. L. Sinclair, "Effects of Particle-Phase Turbulence in Gas-Solid Flows," *AIChE J*., **43**, 853 (1997).
Jackson, R., *The Dynamics of Fluidized Particles*, Cambridge Univ. Press (2000).
Johnson, P.C., Jackson, R., "Frictional-Collisional Constitutive Relations for Granular Materials, with Application to Plane Shearing," *J. Fluid Mech*., **176**, 67 (1987).
Jin,Y., J. X. Zhu, and Z. Q. Yu, "Novel Configurations and Variants," *Circulating Fluidized Beds*, J.R. Grace, A. A. Avidan, and T.M. Knowlton, eds., Blackie Academic & Professionals, London, 525 (1997).
Kashiva, B., and B. VanderHeyden, "Turbulence Theory,"Multiphase Fluid Dynamics Research Consortium, Semi- Annual Meeting and Review, Albuquerque, New Mexico, Apr. 12–14 (2000).
Kuippers J. A. M., B. P. B. Hoomans, and W. P. M. van Swaaij W. P. M., "Hydrodynamic Models of Gas-Fluidized Beds and their Role for Design and Operation of Fluidized Bed Reactors," *Fluidization IX*, L. S. Fan, and T. M. Knowlton, eds., , Engineering Foundation, New York, 15 (1998).
Kwauk. M. W. Ningdre, L. Youchu, C. Bingyu, and S. Zhigun, "Fast Fluidization at ICM,", *Circulating Fluidized Bed Technology*, P. Basu, ed., Pergamon Press, New York, pp 33-–62 (1986).
Matonis, D., D. Gidaspow, and M.Bahary," CFD Simulation of Flow and Turbulence in a Slurry Bubble Column,"*AIChE J.,* **48**, 1413 (2002)
Miller, A. and D. Gidaspow, "Dense Vertical Gas-Solid Flow in a Pipe," *AlChE J.*, **38**, 1801 (1992).
Mudde, R. F., D. J. Lee, J. Reese, and L.-S. Fan, "Role of Coherent Structures on Reynolds Stresses in a 2-D Bubble Column," *AIChE J.,* **43**, 913 (1997).
Neri, A., and D. Gidaspow, "Riser Hydrodynamics: Simulation Using Kinetic Theory," *AIChE J*., **46**, 52 (2000).
Nieuwland, J. J., M. van Sint Annaland, J. A. M. Kuipers, and W. P. M. van Swaaij, "Hydrodynamic Modeling of Gas/Particle Flows in Riser Reactors," *AlChE J.*, **42**, 1569 (1996).
Pan, Y., M. P. Dudukovic, and M. Chang, "Numerical Investigation of Gas-Driven Flow in 2-D Bubble Columns," *AIChE J.,* **46**, 434 (2000).
Pita, J., and S. Sundaresan, "Gas-Solid Flow in Vertical Tubes," *AlChE J.,* **37**, 1009 (1991).
Rhodes, M. J., T. Hiama, G. Cerutti, and D. Geldart, "Non-Unifomities of Solids Flow in Risers of Circulating Fluidized Beds," *Fluidization VI*, J. R. Grace, L. W. Shemilt, and M. A. Bergougnou, eds., Engineering Foundation, New York (1989).
Samuelsberg, A., and B. Hjertager, "Computational Modeling of Gas/Particle Flow in a Riser," *AlChE J*., **42**, 1536 (1996).
Schlichting, H. T., *Boundary-Layer Theory*, Mc Graw Hill, New York (1960).
Seo, Y., and D. Gidaspow, "An X-Ray-Gamma-Ray of Measurement of Binary Solids Concentrations and Void in Fluidized Beds," *Ind. Eng. Chem. Res.,* **26**, 1622 (1987).
Shook, C. A., and M. C. Roco, *Slurry Flow: Principles and Practice*, Butterworth-Heinemann (1991).
Sinclair, J. L., and R. Jackson, "Gas-Particle Flow in a Vertical Pipe with Particle-Particle Interactions," *AlChE J.*, **35**, 1473 (1989).
Sinclair J. L., "Hydrodynamic Modeling," *Circulating Fluidized Beds*, J. R. Grace, A. A. Avidan, and T. M. Knowlton, eds., Blackie Academic and Professionals, 149 (1997).
Smith, P. and S. Kumar, "General Formulation for Multi-Material Flows of Droplets, Particles & Purely Continuous Materials," Multiphase Fluid Dynamics Research Consortium, Semi- Annual Meeting and Review, , Albuquerque, NM (Apr. 12–14, 2000).
Squires. A. M., M. Kwauk, and A. A. Avidan, "Fluid Beds: At Last, Challenging Two Entrenched Practices,"*Science*, **230**, 4732, 1329 (1985).
Strumendo, M., and P. Canu, "Method of Moments for the Dilute Granular Flow of Inelastic Spheres," *Physical Review E*, **66,** 041304 (2002).
Strumendo, M., P. Canu, and D. Gidaspow, " Method of Moments for Dilute Granular Flow: Application to Risers," MFDRC Meeting, Ann Arbor, MI June (2003) and AIChE Meeting, Poster Session on Particle Technology (2003).
Sun, B. and W. J. Koves, "Application of a Numerical Hydrodynamic Model in FCC Design", *AIChE Symp. Series Vol. II,* Miami Beach, FL, 469, (Nov. 15–20, 1998).
Sundaresan, S., "Role of Meso-Scale Structures on Gas-Particle Flows," Multiphase Fluid Dynamics Research Consortium, Semi- Annual Meeting and Review, Albuquerque, NM (Apr. 12–14, 2000).
Tartan, M., "Fluidization in A Riser: Granular Temperature and Stresses," PhD Thesis, Illinois Institute of Technology, Chicago, IL (2003).
Tartan, M., and D. Gidaspow, "Measurement of Radial Granular Temperature Distribution in Risers: Comparison to an Analytical Solution," AIChE Meeting*,* Indianapolis, IN No. 140e (2002).
Therdthianwong, A., and D. Gidaspow, "Hydrodynamics & S02 Sorption in a CFB Loop," *Circulating Fluidized Bed Technology IV*, A. A. Avidan, ed., AlChE, New York, p. 351 (1994).
Thompson, T., Organizer, Dow Chemical Company, Multiphase Fluid Dynamics Research Consortium, E-mail: tbthompson@dow.com, Website: http://www.cpcfd.org/mfdrc,.
Tsuji, Y., Y. Morikawa, and H. Shiomi, "LDV Measurements of an Air-Solid Two Phase Flow in a Vertical Pipe," *J. Fluid Mech.*, **139**, 417 (1984).
Tsuji, Y., T. Tanaka, and S. Yonemura, " Cluster Patterns in Circulating Fluidized Beds Predicted by Numerical Simulation (Discrete Particle Model Versus Two-Fluid Model)," *Powder Technol.*, **95**, 254 (1998).
Tsuo, Y.P. and D. Gidaspow, "Computation of Flow Patterns in Circulating Fluidized Beds," *AIChE J*., **36**, 885 (1990).
Van den Moortel, T., E. Azario, R. Santini, and L. Tadrist, "Experimental Analysis of the Gas-Particle Flow in a Circulating Fluidized Bed Using a Phase Doppler Particle Analyzer," *Chem. Eng. Sci*., **53**, 1883 (1998).
Weinstein, H., M. Shao, M. Schnitzlein, and R., K Graff, "Radial Variation in Void Fraction in a Fast Fluidized Bed," *Fluidization V*, I. C. Ostergaard, and K Sorensen, eds., Engineering Foundation, 329 (1986).
Werther, J., E. -U. Hartge, and D. Rensner, "Measuring Techniques for Gas/Solid Fluidized Bed Reactors," *Chem. Eng. Tech.,* **62**, 605 (1990).
Yerushalmi, J., "High Velocity Fluidized Beds", Chapter 7, *Gas Fluidization Technology*, Chapter 7, D. Geldart, ed., Wiley, New York (1986).
Zhang, D. Z., and W. B. VanderHeyden, "High-Resolution Three-Dimensional Numerical Simulation of a Circulating Fluidized Bed," *Powder Technol.*, **116**, 133 (2001).
Zhang, D. Z., and W. B. VanderHeyden, "The Effects of Mesoscale Structures on the Macroscopic Momentum Equations for Two-Phase Flows," *Int. J. of Multiphase Flow*, **28**, 805 (2002).
Zhang, Y-F., Y. Yang, and H. Arastoopour, "Electrostatic Effect on The Flow Behavior of a Dilute Gas/Cohesive Particle Flow System," *AlChE J.*, **42**, 1590 (1996).

Manuscript received Jan. 3, 2003, and revision received Dec. 11, 2003.